Theoretical Modeling of Prion Disease Incubation

R. V. Kulkarni,* A. Slepoy,† R. R. P. Singh,* D. L. Cox,* and F. Pázmándi*
*Department of Physics, University of California, Davis, California; and †Sandia National Laboratories, Albuquerque, New Mexico

ABSTRACT We apply a theoretical aggregation model to laboratory and epidemiological prion disease incubation time data. In our model, slow growth of misfolded protein aggregates from small initial seeds controls the *latent* or *lag* phase; aggregate fissioning and subsequent spreading leads to an exponential growth phase. Our model accounts for the striking reproducibility of incubation times for high dose inoculation of lab animals. In particular, low dose yields broad incubation time distributions, and increasing dose narrows distributions and yields sharply defined onset times. We also explore how incubation time statistics depend upon aggregate morphology. We apply our model to fit the experimental dose-incubation curves for distinct strains of scrapie, and explain logarithmic variation at high dose and deviations from logarithmic behavior at low dose. We use this to make testable predictions for infectivity time-course experiments.

INTRODUCTION

Understanding the factors which regulate the incubation times for infectious prion diseases is important for assessing the risk of illness after potential exposure as well as for developing treatments which can delay disease onset. There are several striking aspects to prion disease incubation, which are not well-understood.

The incubation times can run into years and decades (Prusiner et al., 1982), and yet, at the laboratory scale have been found to be highly reproducible. In fact, the reproducibility of incubation times with dose has been used as an independent measure of infectivity titer (Prusiner et al., 1982, 1999).

There seem to be distinct stages for the disease incubation after intracerebral inoculation: after rapid initial clearance, there is a *lag phase* (also termed *zero phase*; see Dickinson and Outram, 1979; Kimberlin and Walker, 1988) during which there is little or no infectivity, and an exponential growth or doubling phase, during which the infectivity increases exponentially with a well-defined doubling period (Manuelidis and Fritch, 1996; Bolton, 1998; Beekes et al., 1996). Understanding the lag phase is clearly important as any treatment strategy is more likely to succeed before the exponential growth phase takes over.

As the dose of infection is increased in the laboratory, the incubation times become sharply defined and saturate to a dose-independent value. Below this saturation dose, the incubation time shows a logarithmic dose dependence and at low dose the distribution becomes broad and deviations from logarithmic behavior are observed (Mclean and Bostock, 2000). Such a broad distribution has also been found in epidemiological studies of bovine spongiform encephalopathy (BSE) in England (Stekel et al., 1996; Anderson et al., 1996).

For infection across species, there is a species barrier, and the first passage takes considerably longer to incubate than subsequent passages (Kimberlin and Walker, 1977, 1978).

While prion aggregation has been observed in vitro, the aggregates are neurotoxic but not infectious (Post et al., 2000). These are the issues which motivate our study.

The purpose of this article is to test the extent to which a purely physicochemical model can capture the main reproducible features of prion disease incubation. In particular, we emphasize the importance of the aggregate morphology in determining the statistics of incubation times. Our basic hypothesis is that the lag phase is determined by growth of misfolded protein aggregates from initial small seeds (acquired through infection) to a typical fissioning dimension, whereas subsequent aggregate fissioning and spreading leads to exponential growth and the doubling phase. For a single seed, the lag phase develops a broad but well-defined distribution, which we can calculate via a microscopic statistical model. Thus, when the infection is very dilute, there is a broad distribution of incubation times. At higher doses of infection, self-averaging due to independent growth from many seeds leads to sharply defined incubation times. The dose dependence and its saturation, as well as the ratio of lag time to doubling time depends on the morphology of the aggregates, i.e., whether one has linear fibrils or compact higher-dimensional aggregates. In this sense, details of incubation time distributions provide an indirect means to infer early growth morphologies. Alternative theoretical models which deal with the above issues have also been developed in the literature (Eigen, 1996; Nowak et al., 1998; Masel et al, 1999, Masel and Jansen, 2000; Stumpf and Krakauer, 2000; Payne and Krakauer, 1998; Kellershoh and Laurent, 2001).

The extent to which such a model explains the experimental phenomenology would help address the following questions:

Submitted July 26, 2002, and accepted for publication March 20, 2003.

Address reprint requests to R. V. Kulkarni, Tel.: 609-951-2888; Fax: 609-951-2496; E-mail: kulkarni@physics.ucdavis.edu.

R. V. Kulkarni's present address is NEC Laboratories America, 4 Independence Way, Princeton, NJ.

0006-3495/03/08/707/12 $2.00

Are the incubation times dominated by the nucleation and growth of misfolded protein aggregates?

Are the two phases of prion disease incubation, the lag phase and the exponential growth phase, controlled by the same process, i.e., aggregation of misfolded proteins?

Assuming that aggregate growth controls the incubation timescales, we are led to ask, what is the aggregate morphology during early growth and how does it influence the dose-incubation curves?

Does current data inform us about the characteristic size of the aggregates?

Employing statistical simulations of prion aggregation (based upon cellular automata rules) we argue here that several features of prion disease can be explained by exploring the statistics of the two phases of the disease incubation. Within our model, we show that compact two-dimensional aggregates can provide the observed broad distribution of incubation times for dilute doses and at the same time account for the typical large difference between lag time and doubling time. We present analytic calculations which provide a functional form for the distribution that can be used in further epidemiological studies, and we use these results to infer the dose dependence of the incubation time. Furthermore, our analysis shows how the dose-incubation curve can be related to experimental measurements of the time course of infectivity and in particular, testable predictions can be made using our model for the dose dependence of the lag phase. Finally, we apply our model to epidemiological data for BSE (mad cow disease), from which we conclude that within the model the incubation time is dominated by slow aggregation from a few small (tens of nm scale) starting seeds. This size scale of these seeds is comparable in small animals, but the estimated attachment rates are slower by an order of magnitude or more.

We organize our article as follows: A Model Distribution and Dose-Incubation Curves discusses a model incubation time distribution, which illustrates how our basic picture relates to dose-incubation curves in prion diseases. The sections Cellular Automata Simulations, Stochastic Analysis of Aggregation, and Aggregate Fissioning deal with microscopic models related to protein misfolding, aggregation, and fissioning. In the sections Dose-Incubation Curve, Connection to Epidemiological Data, and Discussion, we come back to the dose-incubation curves, connections to epidemiological data, and the disease phenomenology, and discuss them in the context of our models and present our conclusions.

A MODEL DISTRIBUTION AND DOSE-INCUBATION CURVES

We first illustrate the bare bones of our proposed picture for prion disease incubation by using a model distribution, where calculations can be done analytically. As mentioned in the previous section, our assumption is that the lag phase corresponds to aggregation of misfolded prions from the initial seed up to a fissioning size. This is a stochastic process and, correspondingly, there will be a distribution of aggregation times. Subsequent to this aggregation, we assume (based upon experimental observations) that the number of seeds increases exponentially with a well-defined doubling time (t_2). This exponential growth continues until the number of seeds reaches a critical value which signals the onset of clinical symptoms and the end of the incubation period. We note that this critical value depends on the particular strain of prion disease, inasmuch as different strains target different areas of the brain and can correspondingly cause differing amounts of damage in the target tissue.

In this section, to illustrate the key ideas, we consider an oversimplified (but analytically soluble) model of the aggregation time distribution $P(t)$ associated with a single seed which is uniform on the interval $t_0 \le t \le t_0 + T$:

$$P(t) = 0 \quad t < t_0 \tag{1}$$

$$= \frac{1}{T} \quad t_0 < t < t_0 + T \tag{2}$$

$$= 0 \quad t > t_0 + T. \tag{3}$$

It is useful for what follows to set $T = n_1 t_2$, which measures T in units of the doubling time.

Our simple model assumes that when there are many seeds present, each initial seed will start fissioning into two new seeds after an aggregation time sampled from the above distribution. We will assume that once a seed has fissioned once, it continues to fission or effectively double in a time t_2, which is independent of the above distribution. The microscopic basis for this assumption will be explained in Aggregate Fissioning. The incubation time is given by the mean time taken for a given initial number of seeds (D_i) to reach a critical number (D_f) which is characteristic of when clinical symptoms arise for a given strain.

The dose dependence of the incubation time is then calculated through the following steps:

1. First, we calculate the mean first-arrival time, i.e., the mean time taken for the first aggregate fissioning event. Let the cumulative probability for the first-arrival time for D_i seeds be given by $F^{(D_i)}(t)$. Since each seed grows independently, this can be related to the cumulative probability for the first-arrival time for a single seed via the relation

$$F^{(D_i)}(t) = 1 - (1 - F^{(1)}(t))^{D_i}. \tag{4}$$

The mean first-arrival time t_1 is given by solving $F^{(D_i)}(t_1) = 1/2$. For the simple probability distribution

discussed above, the mean first-arrival time is well-approximated by the expression

$$t_1(D_i) = t_0 + \frac{n_1}{2D_i} t_2. \quad (5)$$

Note that, for a single seed, $t_1 = t_0 + n_1 t_2/2$ is the mean of the distribution $P(t)$, whereas as D_i becomes large, t_1 tends to t_0, i.e., seeds begin to arrive at the onset of the distribution.

2. We now proceed to calculate the time spent in the doubling phase, i.e., the time taken until the number of seeds reaches D_f. All the aggregates formed after fissioning are assumed to further fission in time t_2. Besides these, initial seeds continue to arrive, i.e., aggregate to the fissioning size and thus join the number of seeds that are doubling. The number of initial seeds that arrive during one doubling time interval t_2 is given by $\mathrm{int}(D_i/n_1)$, where $\mathrm{int}(x)$ refers to the integer part of x. Let n_2 be the number of doubling steps needed for the number of seeds to reach the final number D_f. The number of seeds generated after n_2 doubling steps is approximately given by $2^{n_2}(1+\mathrm{int}(D_i/n_1))$. Thus the number of doubling steps n_2 is given by

$$n_2 = \log_2(D_f) - \log_2\left(1 + \mathrm{int}\left(\frac{D_i}{n_1}\right)\right). \quad (6)$$

3. The mean incubation time, which is the sum of the lag-phase time and the doubling phase time, is now given by

$$t_i = t_1(D_i) + n_2 t_2 = t_0 + \frac{n_1}{2D_i} t_2 + \left[\log_2(D_f) - \log_2\left(1 + \mathrm{int}\left(\frac{D_i}{n_1}\right)\right)\right] t_2. \quad (7)$$

The above equation gives the dose dependence of the incubation time for the model distribution. It should be noted that this expression already explains several generic features seen in experimental dose-incubation curves (DICs) and in the microscopic models we present in later sections. These are logarithmic dose dependence at high doses and deviations from logarithmic behavior at low doses. From the above expression for the incubation time, it can be seen that the dominant contribution to the incubation time at high D_i comes from the doubling phase which gives a logarithmic dose dependence. However at low doses ($D \leq n_1$), the time spent in the doubling phase does not change appreciably with dose. Instead, the variation in the incubation time comes from the dose dependence of the first-arrival time, i.e., the lag-phase time. This is reflected as a deviation from the logarithmic behavior in the DIC which is seen in experimental DICs (Prusiner et al., 1980). Our model thus makes the testable prediction that deviations from logarithmic behavior in the DIC should correspond to increases in the lag phase.

We now proceed to develop microscopic models for the initial aggregation process. The next section discusses the cellular automata approach to this problem.

CELLULAR AUTOMATA SIMULATIONS

Theoretical modeling of incubation times (Nowak et al., 1998; Eigen, 1996; Harper and Lansbury, 1997) starting at the molecular level is all but impossible with a 20 order-of-magnitude span between molecular motion timescales and those of disease onset. On the other hand, kinetic theory allows one to model long-time processes but ignores short distance spatial fluctuations, important in nucleation and growth. We have developed a lattice-based, protein-level cellular-automata approach, which bridges these two methodologies (Slepoy et al., 2001). Previously, we used it to calculate aggregation-time distributions, which compared favorably with the incubation times inferred from BSE data (Stekel et al., 1996; Anderson et al., 1996). We also showed that playing with the rules in such simple models can be a cheap way to suggest, constrain, and guide treatment protocols.

Our models consist of dilute concentrations of proteins diffusing on the lattice and interconverting between their properly folded state (PrP^c) and the misfolded state (PrP^{Sc}) (Cohen and Prusiner, 1998) with certain stochastic rules. Even though we employ very simple rules for the interconversion, from our basic understanding of statistical mechanics, we expect the long-time behavior to be modeled correctly. The motivation for our rules is the role of surrounding water molecules in determining the protein conformation. We assume that a monomer isolated from others (surrounded by water molecules) stays in its properly folded state. However, when proteins are surrounded by other proteins, thus excluding water from parts of their neighborhood, they can change conformations and go into a misfolded state (involving β-sheet bonding). A key parameter of our model is the coordination, q_c, at which the misfolded conformation PrP^{Sc} becomes stable. Only misfolded monomers may remain stably in a cluster, possibly breaking away from a cluster when they fold back into the PrP^c form. Note that our model does not discount the influence of other factors in driving the transition from PrP^c to Prp^{Sc}. Our aim is to understand how the aggregation process changes with q_c, which we proceed to do in the following.

Assuming aggregation happens on the cell surface, we choose a two-dimensional hexagonal lattice. The lattice structure and the detailed protein motion are not crucial in our model. At each time step, proteins can move randomly by at most a unit lattice spacing. The magnitude of the time step is set by the time for a single monomer to misfold. It is implicitly assumed that proteins coadsorb with each other followed either by a conversion in shape or separation. It is this conversion process that sets the unit of time.

By playing with the cellular automata rules it is possible to get different aggregate morphologies and aggregation time distributions. First, we consider the case where proteins are isotropic objects. We have performed a large number of runs at values of $q_c = 1$, 2, and 3, with different monomer concentrations (held fixed during the simulation). The aggregation time is defined as the time required to grow from initial seed of size $\mathcal{A}_i$ to a final size $\mathcal{A}$. We always choose the initial seed size to be the minimally stable oligomer of misfolded proteins for a given coordination rule; for $q_c = 1,2,3$, then $\mathcal{A}_i = 2,3,10$. Note that for $q_c = 3$, the $\mathcal{A}_i = 7$ seed is also stable, but possesses a likely spurious trimer-limited attachment barrier to pass to size aggregate size $\mathcal{A}_i = 10$. For a very wide range of concentrations, the lower coordination rules effectively remove the nucleation barrier, leading to frequent nucleation of new clusters. Typical aggregate configurations (and stable seeds) are shown in Fig. 1.

From these studies, we see that lowering the critical coordination provides too rapid a growth for prion aggregates over a wide concentration region, and with no nucleation barrier at these concentrations. In contrast, for $q_c = 3$, the aggregation is very slow and it is characterized by a broad incubation time distribution, with a clear separation in timescales for seeded and unseeded (i.e., infectious and sporadic) cases.

We can also obtain one-dimensional fibril growth by considering the proteins to be anisotropic. For example, on a square lattice, we can get fibrils by: *i*), identifying a preferred bonding face to our simple point proteins, now made into squares. *ii*), We choose a critical coordination of 2. *iii*), We make edge bonding of proteins with adjacent preferred faces to be quite strong under coordination $q = 1$ (i.e., the conversion probability is >50%), and somewhat less strong for face-to-face meeting of proteins. We assume zero conversion probabilities for all other faces. By choosing three kinds of faces with appropriate rules, we can obtain equivalent results on the hexagonal lattice. These rules assure fibril growth which is dimer dominated (see Fig. 1).

STOCHASTIC ANALYSIS OF AGGREGATION

In the low concentration limit, the aggregation results from a sequential addition of proteins to the initial seed. However, addition of monomers is not always stable. Given the rules, various stages of the aggregate size and shape require a pair of proteins (a dimer) to arrive simultaneously, to attach in a stable manner. Thus, the entire process can be approximated by one of stochastic sequential addition of monomer and dimer units. As the concentration, c, goes to zero, the monomer addition rate is proportional to c, whereas the dimer addition rate is proportional to c^2, and thus the growth will involve a minimum number of dimers and these will provide the dominant contribution to the growth times.

The growth to a final size $\mathcal{A}$ from an initial size $\mathcal{A}_i$ involves sequential addition of n units. The probability for the successive additions at intervals $t_1, t_2, \ldots, t_n$ is

$$P(t_1, t_2, \ldots, t_n) = \prod_{j=1}^{n} p_j e^{-p_j t_j}, \tag{8}$$

where the rate for the jth unit, p_j, depends on the geometry of the aggregate and the kind of unit (monomer or dimer) to be added. Hence, the probability distribution associated with the total growth time is

$$P(t) = \int_0^\infty dt_1 \ldots \int_0^\infty dt_n \prod_{j=1}^{n} p_j e^{-p_j t} \delta\left(t - \sum_{i=1}^{n} t_i\right). \tag{9}$$

This integral can be evaluated by standard methods for arbitrary p_i. We note the answers for two cases:

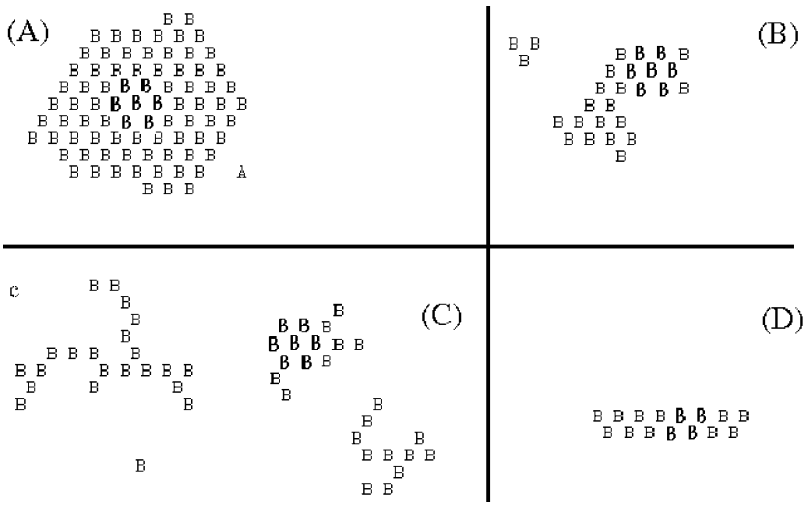

FIGURE 1 Morphologies of seeds (*bold B*s) and corresponding aggregates due to the different rules: (*A*) $q_c = 3$, (*B*) $q_c = 2$, (*C*) $q_c = 1$, and (*D*) fibril growth (see text).

1. The attachment probabilities are identical for each unit, i.e., $p_j = p$ for all j. In this case the probability distribution is the γ-distribution,

$$P(t) = \frac{p(pt)^{n-1}}{(n-1)!}e^{-pt}. \quad (10)$$

2. The rate, $p_j = p + jp'$, increases linearly with j. In this case we obtain the β-distribution in e^{-t} (Szabo, 1988),

$$P(t) = Ae^{-(p+p')t}(1 - e^{-p't})^{n-1}. \quad (11)$$

In one-dimensional fibril growth, dimers are attached one by one with the area available for attachment of dimers staying constant, and thus Eq. 10 applies. For two-dimensional compact growth, slow dimer attachments have to be combined with rapid filling up of rows by monomers. In the low concentration limit, the rate is limited by dimer attachment probabilities which increase linearly with the number of dimers already attached, thus leading to Eq. 11.

At finite concentrations, the monomer attachment times can no longer be neglected, and a more accurate treatment of the timescales in the two-dimensional case requires a convolution of probabilities for monomer attachment times with those for dimer attachment times. The geometrical counting of number of monomers and number of dimers needed to grow to the desired size is straightforward. For the monomers, the distribution of net attachment time is given by the Gamma distribution, i.e., Eq. 10 above, whereas for the dimers it is given by Eq. 11. Since the dimer and monomer attachment times can be taken as independent random variables, the distribution of the total attachment time is given by a convolution of the monomer and dimer probability distributions. The functional form thus obtained can be used to develop accurate fits to the numerical data, as shown in Fig. 2 *A*.

An important aspect of our two-dimensional model is the asymptotic compression of the distributions at low concentrations. The initial stage of the growth is extremely slow and the process speeds up significantly as the aggregate grows. Thus, the mean aggregation time, t_m, to go from an initial seed $\mathcal{A}_i$ to a final size $\mathcal{A}$, can be much larger than the typical aggregate-doubling time, t_2, to go from size $\mathcal{A}/2$ to $\mathcal{A}$. Fig. 3 shows the ratio t_2/t_m for different concentrations and different final sizes $\mathcal{A}$. The crossover to monomer-dominated behavior $(t_2/t_m \approx 1/2)$ is indicated at the highest concentration, whereas at low concentrations this ratio can be much smaller.

AGGREGATE FISSIONING

Fissioning of aggregates leads to exponential growth as the fission products provide seeds for the next round of aggregation. In this subsection, we consider two mechanistic models of the fission process associated with either proteolytic cleavage of aggregates or mechanically induced breakage. We acknowledge that other models are possible (such as continuous fissioning from the aggregate or multiple

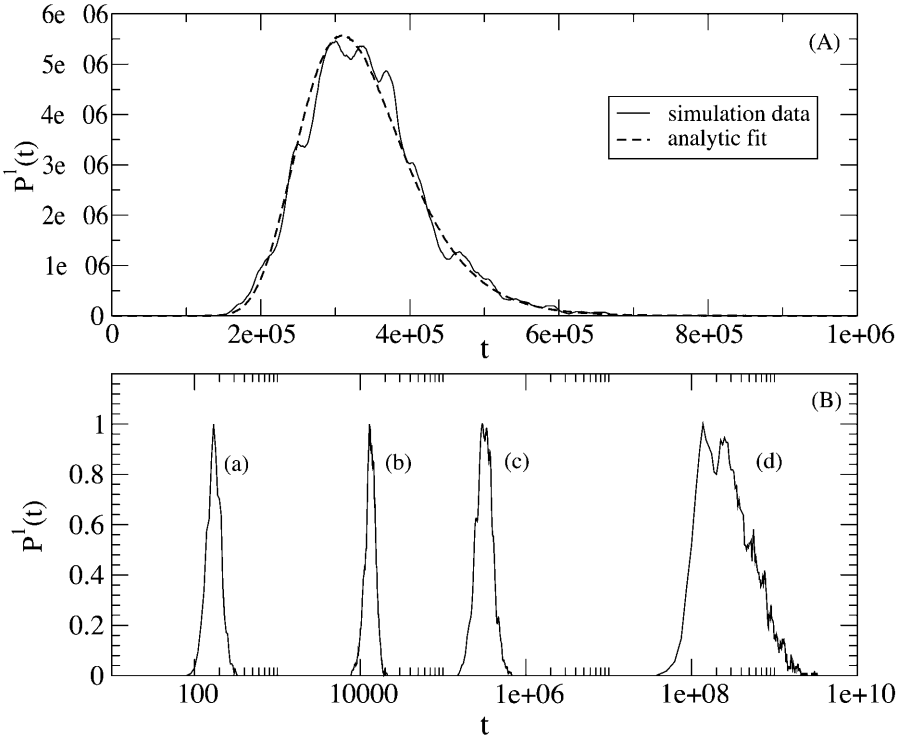

FIGURE 2 (*A*) Comparison of simulation data for single seed aggregation ($\mathcal{A}_i = 10$, $\mathcal{A} = 80$, and $c = 0.2\%$) and fit using analytical calculations (see text) for two-dimensional growth with $q_c = 3$. The unit of time is 1 simulation sweep. (*B*) Probability distributions for (*a*) $q_c = 1$, (*b*) $q_c = 2$, (*c*) $q_c = 3$, and (*d*) sporadic (i.e., with no initial seed) with $q_c = 3$ at the same concentration ($c = 0.2\%$). The maximum probability for all distributions is scaled to unity. The sporadic result is obtained by scaling the data at $c = 1\%$ with an empirically determined c^{-3} factor.

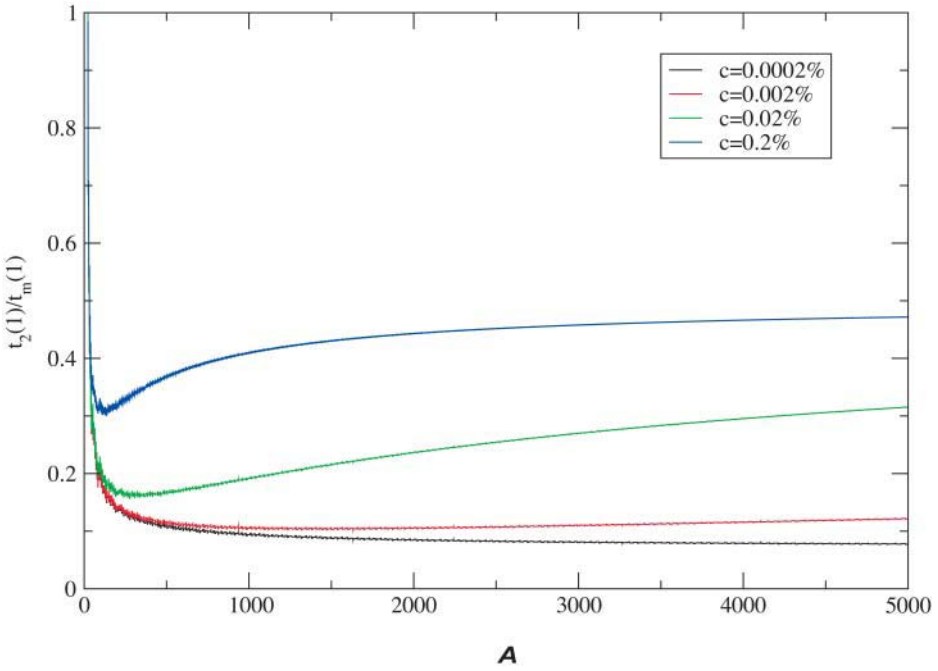

FIGURE 3 Ratio of characteristic doubling time (t_2) to mean incubation time (t_m) as a function of fissioning size $\mathcal{A}$ for single seed growth in two dimensions for different monomer concentrations, showing asymptotic compression as $c \to 0$.

seed fissioning), and we shall discuss these briefly at the end of the section.

We assume that the time required to fission an aggregate (i.e., to actually split it up) is small compared to the aggregation time. This implies a narrow distribution of fission sizes peaked, say, at aggregate size $\mathcal{A}$, and in this limit our results are expected to be independent of the width of the fission distribution.

We consider two extreme limiting models of fission:

Mechanical. In this case, once the aggregate reaches fission size $\mathcal{A}$, it splits into two fragments of equal size $\mathcal{A}/2$. This should approximately describe the situation in which aggregate size is limited by nerve cell curvature, for example (i.e., aggregation favors flat planar or linear structures, but the curvature of the neuron tends to favor curved structures).

Physiological. In this case, the aggregate can break into all smaller lengths at the fission scale. This mimics the outcome of protease attack for which there is no obvious preferred site for breakage.

We take a fixed background concentration of monomers, which should be reasonable for at least short times in the infection time course. The kinetic equation for the time evolution of aggregates with size n (measuring the number of dimers present) and concentration $[a_n]$ is, for $n < \mathcal{A}$,

$$\frac{d[a_n]}{dt} = p_{n-1}[a_{n-1}] - p_n[a_n] + p_{f,n}[a_{\mathcal{A}}], \tag{12}$$

and, for $n = \mathcal{A}$,

$$\frac{d[a_{\mathcal{A}}]}{dt} = p_{\mathcal{A}-1}[a_{\mathcal{A}-1}] - p_{f0}[a_{\mathcal{A}}]. \tag{13}$$

Here, for one-dimensional aggregation $p_n = p_0$, whereas for the two-dimensional aggregation specified by our three critical coordination rules discussed in Cellular Automata Simulations, $p_n = p + np'$. For mechanical fission, $p_{f,n} = 2p_{f0}\delta_{n,\mathcal{A}/2}$, whereas for the physiological fission, $p_{f,n} = 2p_{f0}/(\mathcal{A} - 1)$. The instantaneous fission assumption requires $p_{f,0} \gg p, p'$. In what follows, for the two-dimensional case we fix $p = 2p'$, corresponding to an initial seed of size 10 for which there are two locations to attach a dimer. For large $\mathcal{A}$, these results are insensitive to the choice of p'.

We can identify the doubling time from Eqs. 12 and 13 by the following procedure: first, Laplace transform the set of coupled equations to obtain a matrix equation in transform space, then identify the largest real and positive eigenvalue of the Laplace matrix. In all cases, we find but one real and positive eigenvalue. We have systematically varied the fission size $\mathcal{A}$ and studied the dependence of the exponential growth rate upon fission time. For fibrils, the mean time to aggregate to size $\mathcal{A}$ is $t_m \approx \mathcal{A}/p$, while for the two-dimensional aggregates, the mean aggregation time goes as $t_m \approx \ln(\mathcal{A})/p'$. In the one-dimensional case, we find that for large $\mathcal{A} \geq 10$, the doubling time t_2 tends to $0.5(0.43)t_m$ for mechanical(physiological) fission. Hence, there is but a factor-of-two difference between the aggregation time and the doubling time. Since the numerical difference between mechanical and physiological fission is not substantial, we have examined only the mechanical fission model for the two-dimensional aggregate. In this case, for large $\mathcal{A} \geq 20$, we find that the largest eigenvalue of the Laplace matrix goes as $\simeq 0.4/p'$ independent of $\mathcal{A}$, whereas

the aggregation time-scales as $\ln(\mathcal{A})/p'$. Hence, for sufficiently large $\mathcal{A}$ it is possible to make $t_2/t_m \ll 1$.

These results have the attractive feature of linking the aggregation time, which we associate with the lag phase, to the doubling time in fission. In the one-dimensional case, so long as the fission is binary (two fragments), the roughly factor-of-two difference in t_m and t_2 is very difficult to avoid. However, for the two-dimensional case, it is possible to have a jagged boundary arise after binary fission which allows more rapid aggregation to $\mathcal{A}$ from $\mathcal{A}/2$, so that t_2 calculated in the previous paragraph is an upper bound for mechanical fission.

However, we acknowledge that other processes may be responsible for the fission. In particular, we cannot rule out continuous fissioning of fragments off of large aggregates which may lead to a very different result provided the fission rate is comparable to growth rates.

DOSE-INCUBATION CURVE

In this section, we will look at the total incubation time and how it varies as a function of the inoculated dose using the aggregation-time distributions derived in the previous sections, and explore the extent to which it provides a quantitative description of experimental dose-incubation curves. As discussed before, a key advantage of the two-dimensional growth models is that, with a suitable fissioning scenario, they lead to lag times much larger than doubling times. This is difficult to accomplish with the one-dimensional growth models. However, in this section we will assume that the doubling time is an independent free parameter. This allows us to fit the experimental dose-incubation curves by both one- and two-dimensional models. The constraints on relative values of lag times and doubling times will be brought up in our discussions in the next section.

We now proceed to calculate the incubation time as a function of inoculated dose within our model for both one- and two-dimensional aggregation models and compare with laboratory data. Consider first the DIC of the 263K hamster scrapie strain. Kimberlin and Walker (1986) have determined the DIC along with independent measurements of the doubling time t_2 and the final infectivity for this strain. The doubling time t_2 can also be inferred from the DIC in the region where it shows a logarithmic dose dependence. Besides this experimental data, we need to know the clearance ratio r_i which gives the percentage of the number of infectious seeds in a given inoculum which are removed by rapid initial clearance. Let us illustrate this for the case of 1 LD_{50} unit: in our model this corresponds to having a 50% probability of attaching a single infectious seed. Correspondingly, the initial inoculum has to contain, on average, $50/(100 - r_i)$ seeds (for $r_i > 50\%$, typical values from experiment are $r_i \sim 99\%$; Manuelidis and Fritch, 1996). We treat r_i as a parameter in our model to be determined by fitting the DIC. Using this, in conjunction with our results for the aggregation time distributions, we can generate theoretical DICs using the method outlined in A Model Distribution and Dose-Incubation Curves.

For a fixed aggregation size $\mathcal{A}$, with probability of attachment p and infectivity ratio r_i (which are the parameters we use to fit the DIC), we then calculate the mean-square deviation (S^2) (normalized by the experimental error estimates for each data point) between the theoretical and experimental DICs. Minimizing S^2 gives us the optimal parameters, p and $\mathcal{A}$, for the particular strain for a given value of r_i within our model.

We consider first the DIC for the 263K hamster scrapie strain. In carrying out the fitting, we have ignored the results at the highest doses since in this limit we are approaching the saturation of the incubation time. Thus the data which we are fitting consists of five data points corresponding to five serial 10-fold dilutions. For our two-dimensional growth model, we get a good fit to the experimental data as indicated in Fig. 4 *top*. The optimal parameters in this case are $\mathcal{A} = 16$ (with $\mathcal{A}_i = 10$), $p = 0.025\ \text{day}^{-1}$ and $r_i = 0$ (which seems unphysical) for which $S^2 \sim 0.07$. For a more realistic value of $r_i \sim 88\%$, we get $\mathcal{A} = 16$, $p = 0.16\ \text{day}^{-1}$ with $S^2 \sim 1.14$. From the fitting, one can see that the clearance ratio r_i cannot be much greater than $r_i \sim 88\%$ due to the constraints imposed by the experimental incubation and doubling times. It should be noted, furthermore, that the above procedure does not uniquely determine these parameters since comparably good fits are obtained for higher values of $\mathcal{A}$ by correspondingly adjusting p. For the one-dimensional growth model, we also get a good fit with $S^2 \sim 0.35$ for $\mathcal{A} = 8$ (with $\mathcal{A}_i = 4$) and $p = 0.11\ \text{day}^{-1}$.

One of the unusual features of the 263K scrapie strain in hamsters is that at high doses the lag time is negligibly small. This feature is clearly seen in the time-course measurements (Kimberlin and Walker, 1986) of infectivity and also accords with the theoretical best-fit results described above. To test our procedure for what is arguably a more representative strain, we have also obtained a fit for the experimental DIC for the ME7 strain in C57BL mice (Taylor et al., 2000). This data effectively corresponds to mean incubation times for four serial 10-fold dilutions, ignoring the incubation times at the highest dose which correspond to saturation of the DIC. The results obtained by using our two-dimensional growth model are shown in Fig. 4 *middle*. In this case, the theoretical fit is not as good as that obtained for the 263K strain; the optimal parameters correspond to $\mathcal{A} = 140$, $p = 0.033\ \text{day}^{-1}$ for $r_i = 99$ which gives $S^2 \sim 3.75$. A comparably good fit was obtained by using the one-dimensional growth model with the optimal parameters $\mathcal{A} = 40$, $p = 0.23\ \text{day}^{-1}$ for $r_i = 99$, which gave $S^2 \sim 5.02$. However, in contrast with the 263K strain, the theoretical results for the ME7 strain give rise to a significant lag time of ~50 days for the highest dose inoculated. This is a testable prediction for time-course measurements of infectivity for the Me7 strain in C57BL mice.

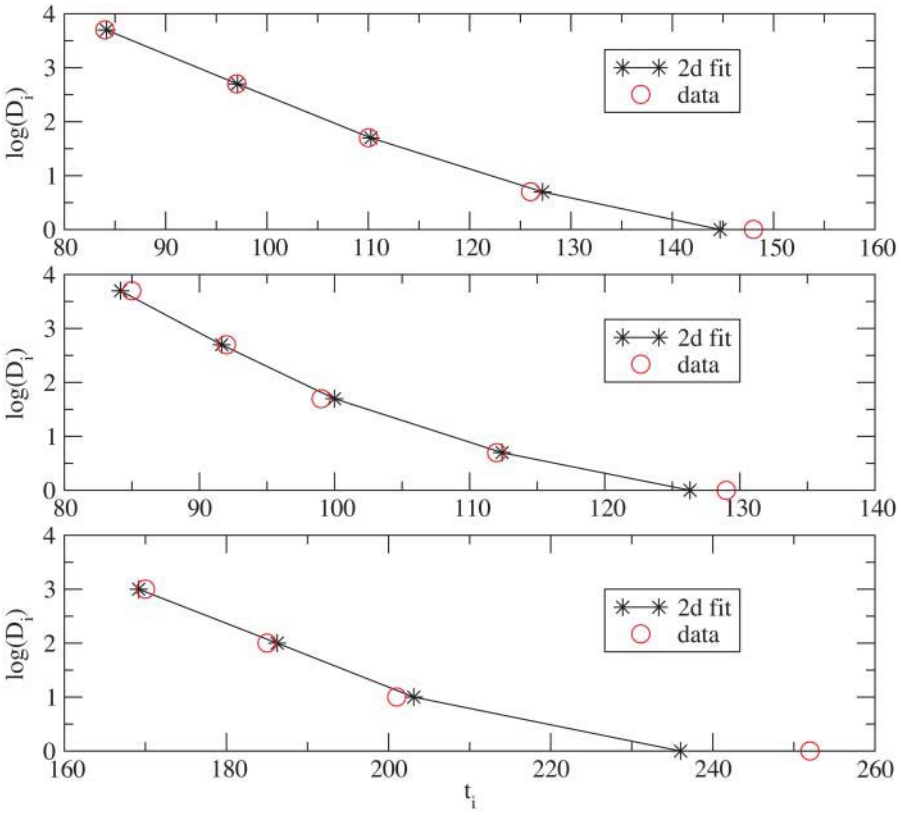

FIGURE 4 (*Top*) Experimental and theoretical dose-incubation curves for the 263K hamster scrapie strain for $r_i = 0$. The *x*-axis shows the incubation time and the *y*-axis shows the logarithm of the number of seeds inoculated. The theoretical curve is the best fit to the experimental data using the two-dimensional growth model for aggregation. (*Middle*) Same as $\mathcal{A}$ but for the Sc237 strain in hamsters with $r_i = 88$. (*Bottom*) Same as $\mathcal{A}$, but for the Me7 strain in C57BL mice with $r_i = 88$.

Finally, we have used the above procedure to analyze the Sc237 scrapie strain in hamsters. In many respects, this strain is similar to the 263K scrapie strain in hamsters; however, an analysis of the respective DICs reveals some significant differences. Based on the best-fit formula for the DIC (Prusiner et al., 1999), we can estimate a doubling time t_2 for the Sc237 strain to be ~2.1 days whereas the doubling time for the 263K strain is ~3.9 days. This difference is also reflected in our theoretical best-fit DIC curve for this strain which, for $r_i = 99$, is given by the parameters $\mathcal{A} = 80$, $p = 0.052\ \text{day}^{-1}$. Note that the experimental data in this case was obtained from the best-fit formula for the DIC (Prusiner et al., 1999) mentioned above. For our one-dimensional model, the corresponding values are $\mathcal{A} = 62$, $p = 0.35\ \text{day}^{-1}$. Note that the experimental data in this case was obtained from the best-fit formula for the DIC (Prusiner et al., 1999). Furthermore, the experimental error estimates were not available for dose-incubation data for this strain, so we assumed them to be the same as that for the 263K strain in determining the best fit. Using the above fits, we see that the theoretical prediction for the mean lag time for an inoculated dose of 1 LD_{50} unit is ~50 days. This value seems to be in good agreement with the experimental results for low dose inoculations for this strain (Prusiner et al., 1999).

The key results from our fitting (using the two-dimensional growth model) are summarized in Table 1. Based on the above results, we conclude that while our model accounts for the features of the DIC and gives a good fit to the experimental data, the latter cannot be used to distinguish between the one-dimensional and two-dimensional growth morphologies or to ascertain the model parameters conclusively. However, despite the ambiguity in the model parameters, there are some robust predictions we can make after fitting the DICs. We find that the experimental DIC, in conjunction with our model, can be used to make predictions for the time course of infectivity: in particular we can predict the lag-time as a function of dose. Although the duration of the lag time that we calculate does depend on the clearance ratio r_i, we note that the trend is that increasing r_i reduces the lag time. Thus by measuring the lag time at high doses we can determine the parameter r_i in our model, which then

TABLE 1 Calculated best-fit parameters and predictions for low dose lag times for three scrapie strains

Strain	t_2 (days)	r_i	Lag time (days)	p' (days^{-1})	$\mathcal{A}$	S^2
263K	3.9*	0	27.7	0.025	16	0.07
		88	4.3	0.16	16	1.14
Sc237	2.1†	88	56.9	0.052	140	0.11
		99	48.9	0.052	80	0.11
Me7	4.5‡	88	107	0.033	360	3.86
		99	89.6	0.033	140	3.75

*Kimberlin and Walker (1986).
†Prusiner et al. (1999).
‡Taylor et al. (2000).

yields testable predictions for the lag time at low doses. In the case of the Sc237 scrapie strain in hamsters, our calculated lag time at low dose agrees well with experimental results for the same. For the other strains, the predictions for the lag time at low dose are a key testable prediction of our model.

CONNECTION TO EPIDEMIOLOGICAL DATA

We have found no dose-incubation time data available for large mammals in the literature, so to gain insight we have analyzed epidemiological data for BSE in cattle (Anderson et al., 1996; Ferguson et al., 1998). In brief, our assumptions and methods are as follows.

Model distribution

We apply only the two-dimensional model in the dilute dose limit (suitable for digested prions); comparable quality fits can be obtained from the one-dimensional model, but the estimated t_2/t_m ratio consistently and strongly violates our mechanistic model result from Aggregate Fissioning, whereas the bound for the two-dimensional case is satisfied.

Number of doublings

For mice and hamsters, with 1-g brains, 30 doublings to incubation is typical (in the low dose limit). Given that the mean cattle brain is 500 g, $\sim 2^9$ times that of mice/hamsters, we take $n_2 = 40$ doublings from infection to incubation for cattle.

BSE fits

Anderson et al. (1996) provide a candidate incubation time distribution which best fits the epidemic time course, and yields a mean incubation time $t_i = 5$ years and standard deviation of 1.3 years. Let us introduce a parameter $l = 1 + p/p'$, which parameterizes the number of ways to attach to the initial seed aggregate (e.g., for $\mathcal{A}_i = 10$ as in the previous section, $l = 3$). Let n be the number of dimers added to reach size $\mathcal{A}$ characteristic of fissioning. We consider variation with n, l here to assess the robustness of our conclusions. The BSE distribution width fixes p' uniquely for given n, l, with p' weakly dependent upon n. We readily calculate the mean first arrival time $t_m(n, l, p') \approx (\psi(n + l) - \psi(l))/p'$ ($\psi(x) = d \ln \Gamma(x)/dx$ is the digamma function), and, as per the discussion in A Model Distribution and Dose-Incubation Curves, we take the difference t_i–t_m to be $n_2 t_2$, the length of the exponential growth phase. We assume that a minimum t_2 value for cattle is the 5 days typical for hamsters and mice (see Table 2). From this, we can find the maximum n value for a given l. By assuming a maximum n-value for small aggregates (plausibly taken as $n = 6$), we generate an upper bound for t_2 of 15 days. The results for $l = 2,10$ are summarized in Table 2. Importantly, we find the maximum aggregate size at fission to be of order 80–100 monomers, approximately independent of l for $2 \leq l \leq 10$.

TABLE 2 Fits to incubation time distribution for BSE

l	n	p' (yrs^{-1})	t_m (yrs.)	t_2 (days)
2	6	0.57	2.8	20
2	23	0.61	4.5	5
10	6	0.15	3.2	16

See Ferguson et al. (1998).

This analysis demonstrates only that the inferred incubation time distribution, for which the width is ~30% of the mean, is compatible with our hypothesis in the low dose limit, and does not rule out variance from other mechanisms. The low dose limit is reasonable for food-based infection. However, other sources of variance may arise, in this limit, from variation in dose, brain and body size, transportation of infection inside the body, etc., and should also be investigated.

An interesting conclusion from the analysis of the BSE data especially is that the doubling times found within our model are quite comparable to those from small animal studies, so that the order-of-magnitude variation in incubation time must be ascribed to slower attachment rates. The strongest control of that for our model is concentration. Given the potential role of prion proteins in limiting oxidative damage of synapses (Guentchev et al., 2002), and the slower metabolic rate of large mammals, it would appear that metabolic regulation of normal prion monomer concentration is an intriguing possibility for further exploration.

DISCUSSION

Recall that our basic hypothesis is that incubation times are controlled by prion aggregation around infectious external seeds on the neuronal surface. Furthermore, in our calculations, the distribution of aggregation times arises from the stochastic growth process from seeds of a given initial size. That only a narrow range of seed sizes is relevant here may be motivated by size sensitivity of the blood-brain barrier, the attachment probability, and the transportability of the seeds. Our basic assumption is that the lag phase corresponds to growth from initial seeds to a characteristic fissioning dimension $\mathcal{A}$, after which one gets a multiplication in seeding centers and an exponential growth in infectivity.

That there is a long lag time despite external seeding by intracerebral inoculation (Manuelidis and Fritch, 1996; Kimberlin and Walker, 1988), and a doubling time which is typically significantly shorter (Manuelidis and Fritch, 1996), both of which become sharply defined at high doses, seems to be a general feature of the prion diseases. Our two-dimensional compact aggregate model, with the assumptions of the preceding paragraph, explains these facts. In par-

ticular, two-dimensional compact aggregation generates a broad distribution of aggregation times for a single seed with a well defined sharp onset time (t_0) and mean aggregation time (t_m). With increasing number of seeds (D_i), the distribution of times for the first seed to reach the typical fissioning size $\mathcal{A}$ will narrow. Correspondingly the lag time, determined by the first fissioning event, will become sharply defined and concentrate at the onset time, which only weakly depends upon D_i.

The doubling time (t_2) is defined by fissioning and subsequent growth from size $\mathcal{A}/2$ to $\mathcal{A}$. Since growth from different seeds is independent, self-averaging gives a sharply defined t_2. Thus at high doses both the lag time and doubling time are sharply defined, which accounts for one of the most striking features of prion diseases: the reproducibility of incubation times at high doses. Indeed, we can explain several features of the dose-incubation curve. Notably, above a saturation dose D_s, the incubation time does not decrease, whereas for $D < D_s$, the incubation time varies as $\log(D)$, showing deviations from the log only below a much smaller value D_{min} (Prusiner et al., 1982; Masel et al., 1999). The total incubation time is the sum of the lag time and $n_d t_2$, where n_d is the number of doubling steps. Assuming that the onset of clinical symptoms is related to the damage of a fixed number of neurons (Nowak et al., 1998), the logarithmic dose dependence of the number of doubling steps follows from the fact that number of seeds grows exponentially in the fissioning stage. In the range $D_{min} < D < D_s$, the lag time does not change appreciably with dose, thereby giving rise to the logarithmic dose dependence of the incubation time in this range. At low doses ($D < D_{min}$), the lag time increases toward $t_m 1$ (the mean aggregation time for a single seed) giving rise to a broad distribution of incubation times and the deviation from the logarithmic behavior in the DIC which is observed experimentally. (Prusiner et al., 1980)

Furthermore, we note that in our mechanistic fissioning model, the doubling time (t_2) is bounded above by the time to grow from size $\mathcal{A}/2$ to $\mathcal{A}$. If the fission produces jagged fragments, these can be effectively filled by monomers which will accelerate the subsequent growth process. This is only possible for two-dimensional compact aggregates and not for one-dimensional fibrils, for which the exposed ends will always be limited to dimer growth. This possibility may account for the effective $1/c$ dependence in the incubation time observed for transgenic mice with multiple copies of the hamster prion protein gene (Prusiner et al., 1990), noting that for hamsters the doubling phase appears to dominate incubation (Kimberlin and Walker, 1986).

A key difference between the one-dimensional and two-dimensional morphology (shown in Stochastic Analysis of Aggregation) is that, within our model, in case of the latter, *i*), the lag time can be an order-of-magnitude larger than the doubling time. If the total time in doubling steps becomes large compared to the lag time, the overall distribution will be relatively narrow. Thus, only in the case of two-dimensional growth can one get *ii*), a wide distribution for the overall incubation time, with a width comparable to the mean. Thus assuming *i*) and *ii*) to result entirely from the growth processes discussed here strongly points to a two-dimensional (or three-dimensional) morphology as controlling the incubation times. It is encouraging to note that recent experiments (Wille et al., 2002) have found the first experimental evidence of hexagonally coordinated two-dimensional prion aggregates.

The early growth morphology clearly deserves further experimental attention (Horiuchi and Caughey, 1999; Rochet and Lansbury, 2000). Typically, the in vitro morphology of prion aggregates has been found to be fibrillar (Ionescu-Zanetti et al., 1999). Frequently large fibrillar aggregates are also observed post mortem in brain tissues. The morphology and size scale for aggregates that cause neuronal death and infection is not known. One could argue that the reason why in vitro aggregates are not infectious is because they do not have the proper morphology. We speculate that the attachment to lipid membranes could make a vital difference to the aggregation process, which is missing in the in vitro experiments. It would be very interesting to carry out the in vitro studies of prion aggregation in presence of lipid membranes.

An important byproduct of our analysis is the ability to predict the time course of infectivity from the DIC. Provided we take the doubling time (t_d) as an independent experimental parameter, such predictions are very robust and do not rely on many details of the aggregation-fissioning model, including initial growth morphologies. Such predictions are particularly significant since experiments which measure the time course of infectivity, and hence determine the lag phase, are extremely expensive and time-consuming. This dose dependence of the lag phase may well be a significant factor in assessing the risk of infection.

Our results indicate that we can infer the (average) time course of infectivity using the information supplied by the experimental DIC. Thus, based on our fits to the experimental DIC, we have made testable predictions for the time course of infectivity, and in particular the lag time, as a function of dose. These predictions are in good agreement with the existing experimental results and their further experimental validation would prove very useful.

A factor which significantly affects the lag time is the probability of dimer attachment p; lowering p increases the lag time. This is relevant in understanding the species barrier effect in which there is a reduction of incubation times with multiple passages in interspecies infection (Lasmézas et al., 1997). During first passage, the attachment of dimers is initially nonhomologous but as the seed size increases it should change to homologous attachment. Since the nonhomologous attachment probability should be smaller (Horiuchi et al., 2000), the lag phase should be longer for first passage as compared to subsequent passages. Thus, in our picture, most of the difference in incubation times should

come from the lag phase and the exponential growth phase should be similar between first and second passages. This has been observed experimentally for hamster scrapie passaged in mice (Kimberlin and Walker, 1978). We note that the estimated dimer attachment rates for mice and hamsters range from 9–60 per year (compare with Table 1), whereas for cattle they are maximally 0.6 per year.

Furthermore, we observe that the estimated aggregate sizes are comparable between large animals (cattle) and small animals, all in the ballpark of tens of nm, which is precisely the estimated size of the lipid rafts on which prions are hypothesized to rest (Simons and Toomre, 2000). The comparable sizes of aggregates at fission we find in our model between small and large mammals strongly suggests that the primary determinant of the lag time is the dimer attachment rate which is regulated primarily by the concentration (for a given strain) within our model. This leads us to speculate that the concentration of normal prion proteins must vary dramatically between large and small species, which naturally leads us to envision a link to metabolic rate. Such a link is plausible if prion proteins play a functional role in relieving oxidative stress as has been proposed elsewhere (Guentchev et al., 2002). It would be of interest to experimentally test this hypothesis of enhanced homeostatic PrP^c concentration in small animals relative to large ones.

In summary, we have explored the statistics of the two phases corresponding to growth of infectivity after intracerebral inoculation. We associate the lag phase with growth of prion aggregates up to a fissioning dimension and explore the consequences of aggregate morphology on incubation time distributions using cellular automata-based models. Our analysis accounts for the striking reproducibility of incubation times at high doses and predicts that the broadening at low doses should be accompanied by increases in the mean lag-phase time. Furthermore, we have presented a general scheme for inferring the dose-incubation curve given the distribution of lag-phase times for individual seeds and the infectivity doubling time. Using the calculated lag-phase distributions for our one-dimensional and two-dimensional growth models, we used this scheme to provide theoretical fits to experimental DICs based on which we make predictions for the time course of infectivity. Finally, we considered the epidemiological data for BSE and showed that, within our model, the aggregate size for BSE is comparable to that for scrapie in smaller animals such as hamsters and mice.

We acknowledge useful discussions with F. Cohen. R.R.P.S. and D.L.C. have benefited from discussions at workshops of the Institute for Complex Adaptive Matter.

R.V.K. and D.L.C. acknowledge support from the U.S. Department of Energy, Office of Basic Energy Sciences, Division of Materials Research. A.S. is supported by Sandia, which is a multiprogram laboratory operated by Sandia Corporation, a Lockheed Martin company, for the United States Department of Energy under Contract No. DE-AC04-94AL85000. We are grateful for a grant of supercomputer time from the Lawrence Livermore National Laboratory.

REFERENCES

Anderson, R. M., C. A. Donnelly, N. M. Ferguson, M. E. J. Woolhouse, C. J. Watt, H. J. Udy, S. M. A. Whinney, S. P. Dunstan, T. R. E. Southwood, J. W. Wilesmith, J. B. M. Ryan, L. J. Hoinville, J. E. Hillerton, A. R. Austin, and G. A. H. Wells. 1996. Transmission dynamics and epidemiology of BSE in British cattle. *Nature*. 382:779–788.

Beekes, M., E. Baldauf, and H. Diringer. 1996. Sequential appearance and accumulation of pathognomonic markers in the central nervous system of hamsters orally infected with scrapie. *J. Gen. Vir.* 77:1925–1930.

Bolton, D. C. 1998. Prion distribution in hamster lung and brain following intraperitoneal inoculation. *J. Gen. Virol.* 79:2557–2562.

Cohen, F. E., and S. B. Prusiner. 1998. Pathologic conformations of prion proteins. *Annu. Rev. Biochem.* 67:793–819.

Dickinson, A. G., and G. W. Outram. 1979. The scrapie replication-site hypothesis and its implications for pathogenesis. *In* Slow Transmissible Diseases of the Nervous System. S.B. Prusiner and W.J. Hadlow, editors. Academic Press, New York. Vol. 2:13–32.

Eigen, M. 1996. Prionics or the kinetic basis of prion diseases. *Biophys. Chem.* 63:A1–A18.

Ferguson, N. M., C. A. Donnelly, M. E. J. Woolhouse, and R. M. Anderson. 1998. The epidemiology of BSE in cattle herds in Great Britain. II. Model constructions and analysis of transmission dynamics. *Phil. Trans. Ser. B R. Soc. Lond.* 352:803–838.

Guentchev, M., S. L. Siedlak, C. Jarius, F. Tagliavini, R. J. Castellani, G. Perry, M. A. Smith, and H. Budka. 2002. Oxidative damage to nucleic acids in human prion disease. *Neurobiol. Dis.* 9:275–281.

Harper, J. D., and P. T. Lansbury, Jr. 1997. Models of amyloid seeding in Alzheimer's disease and scrapie: mechanistic truths and physiological consequences of the time-dependent solubility of amyloid proteins. *Annu. Rev. Biochem.* 66:385–407.

Horiuchi, M., and B. Caughey. 1999. Prion protein interconversions and the transmissible spongiform encephalopathies. *Struct. Fold. Des.* 7:R231–R240.

Horiuchi, M., S. A. Priola, J. Chabry, and B. Caughey. 2000. Interactions between heterologous forms of prion protein: binding, inhibition of conversion, and species barriers. *Proc. Natl. Acad. Sci. USA.* 97:5836–5841.

Ionescu-Zanetti, C., R. Khurana, J. R. Gillespie, J. S. Petrick, L. C. Trabachino, L. J. Minert, S. A. Carter, and A. L. Fink. 1999. Monitoring the assembly of Ig light-chain amyloid fibrils by atomic force microscopy. *Proc. Natl. Acad. Sci. USA.* 96:13175–13179.

Kellershoh, N., and M. Laurent. 2001. Prion diseases: dynamics of the infection and properties of the bistable transition. *Biophys. J.* 81:2517–2529.

Kimberlin, R. H., and C. A. Walker. 1977. Characteristics of a short incubation model of scrapie in the golden hamster. *J. Gen. Virol.* 34:295–304.

Kimberlin, R. H., and C. A. Walker. 1978. Pathogenesis of scrapie: agent multiplication in brain at the first and second passage of hamster scrapie in mice. *J. Gen. Virol.* 42:107–117.

Kimberlin, R. H., and C. A. Walker. 1986. Pathogenesis of scrapie (strain-263K) in hamsters infected intracerebrally, intraperitoneally or intraocularly. *J. Gen. Virol.* 67:255–263.

Kimberlin, R. H., and C. A. Walker. 1988. Pathogenesis of experimental scrapie. *In* Novel Infectious Agents and the Central Nervous System. T. Bock and J. Marsh, editors. Wiley, Chichester. Ciba Foundation Symposium. 135:37–62.

Lasmézas, C. I., J.-P. Deslys, O. Robain, A. Jaegly, V. Beringue, J.-M. Peyrin, J.-G. Fournier, J.-J. Hauw, J. Rossier, and D. Dormont. 1997. Transmission of the BSE agent to mice in the absence of detectable abnormal prion protein. *Science*. 275:402–404.

Manuelidis, L., and W. Fritch. 1996. Infectivity and host responses in Creutzfeldt-Jakob disease. *Virology*. 216:46–59.

Masel, J., and V. A. A. Jansen. 2000. Designing drugs to stop the formation of prion aggregates and other amyloids. *Biophys. Chem*. 88:47–59.

Masel, J., V. A. A. Jansen, and M. A. Nowak. 1999. Quantifying the kinetic parameters of prion replication. *Biophys. Chem*. 77:139–152.

Mclean, A. R., and C. J. Bostock. 2000. Scrapie infections initiated at varying doses: an analysis of 117 titration experiments. *Phil. Trans. R. Soc. Lond. B*. 355:1043–1050.

Nowak, M. A., D. C. Krakauer, A. Klug, and R. M. May. 1998. Prion infection dynamics. *Integr. Biol*. 1:3–15.

Payne, R. J. H., and D. C. Krakauer. 1998. The spatial dynamics of prion disease. *Proc. R. Soc. Lond. B Biol. Sci*. 265:2341–2346.

Post, K., D. R. Brown, M. Groschup, H. A. Kretzschmar, and D. Riesner. 2000. Neurotoxicity but not infectivity of prion proteins can be induced reversibly in vitro. *Arch. Virol*. 16:S265–S273.

Prusiner, S. B., D. F. Groth, S. P. Cochran, F. R. Masiarz, M. P. McKinley, and H. M. Martinez. 1980. Molecular properties, partial purification, and assay by incubation period measurements of the hamster scrapie agent. *Biochemistry*. 19:4883–4891.

Prusiner, S. B., S. P. Cochran, D. F. Groth, D. E. Downey, K. A. Bowman, and H. M. Martinez. 1982. Measurement of the scrapie agent using an incubation time interval assay. *Ann. Neurol*. 11:353–358.

Prusiner, S. B., M. Scott, D. Foster, K.-M. Pan, D. Groth, C. Mirenda, M. Torchia, S.-L. Yang, D. Serban, G. A. Carlson, P. C. Hoppe, D. Westaway, and S. J. DeArmond. 1990. Transgenetic studies implicate interactions between homologous PrP isoforms in scrapie prion replication. *Cell*. 63:673–686.

Prusiner, S. B., P. Tremblay, J. Safar, M. Torchia, and S. J. DeArmond. 1999. Bioassays of Prions. *In* Prion Biology and Diseases. S. B. Prusiner, editor. Cold Spring Harbor Laboratory Press, Cold Spring Harbor, NY. pp.113–145.

Rochet, J. C., and P. T. Lansbury. 2000. Amyloid fibrillogenesis: themes and variations. *Curr. Opin. Struc. Biol*. 10:60–68.

Simons, K., and D. Toomre. 2000. Lipid rafts and signal transduction. *Nat. Rev. Mol. Cell Biol*. 1:31–39.

Slepoy, A., R. R. P. Singh, F. Pazmandi, R. V. Kulkarni, and D. L. Cox. 2001. Statistical mechanics of prion diseases. *Phys. Rev. Lett*. 87:058101.

Stekel, D. J., M. A. Nowak, and T. R. E. Southwood. 1996. Prediction of future BSE spread. *Nature*. 381:119.

Stumpf, M. P. H., and D. C. Krakauer. 2000. Mapping the parameters of prion-induced neuropathology. *Proc. Natl. Acad. Sci. USA*. 97:10573–10577.

Szabo, A. 1988. Fluctuations in the polymerization of sickle hemoglobin—-a simple analytic model. *J. Mol. Biol*. 199:539–542.

Taylor, D. M., I. McConnell, and C. E. Ferguson. 2000. Closely similar values obtained when the Me7 strain of scrapie agent was titrated in parallel by two individuals in separate laboratories using two sublines of C57BL mice. *J. Virol. Meth*. 86:35–40.

Wille, H., M. D. Michelitsch, V. Guenebaut, S. Supattapone, A. Serban, F. E. Cohen, D. A. Agard, and S. B. Prusiner. 2002. Structural studies of the scrapie prions protein by electron crystallography. *Proc. Natl. Acad. Sci. USA*. 99:3563–3568.